Ceramics International xxx (xxxx) xxx–xxx

Contents lists available at ScienceDirect

Ceramics International

journal homepage: www.elsevier.com/locate/ceramint

From sub-microsized $MgAl_2O_4$ powder to $MgAl_2O_4$-Si_3N_4 nanocomposite powder by spray drying of ultrasonicated suspensions

M.R. Loghman-Estarki[a,*], H. Sheikh[a,*], E. Mohammad sharifi[a], M.H. Babaee[b], M. Kharraziha[b], A. Alhaji[a]

[a] Department of Materials Engineering, Malek Ashtar University of Technology, Shahin Shahr, Isfahan 83157-13115, Iran
[b] Department of Materials Engineering, Isfahan University of Technology, Isfahan 84156-83111, Iran

ARTICLE INFO

Keywords:
Ultrasonic irradiation
Nanocomposite
Granules

ABSTRACT

The prime objective of this work is an investigation on the effect of ultrasonic processing and suspension formulation including the amount of the binder and the dispersant agent on the morphology, circularity factor, and flowability of the resulting granules. In order to do so, the $MgAl_2O_4$–2.5vol%Si_3N_4 suspension was firstly prepared with ultrasonic irradiation of $MgAl_2O_4$-Si_3N_4 nanoparticles in distilled water with the assistance of a dispersant agent (Dolapix CE 64) and PVA (poly vinyl alcohol) binder. Then, the nanocomposite granules were produced by spray drying of the suspension. The characterizations of the initial powders and the obtained granules were studied by X-ray diffraction (XRD), Fourier transform infrared spectroscopy (FTIR), scanning electron microscopy (SEM) analyses. The results showed that the ultrasonic treatment can break the initial agglomerated spinel powders into a fine distribution of particle size. Also, spray drying of the ultrasonic-treated suspension can produce granules with desirable morphology and flowability.

1. Introduction

Magnesium aluminate ($MgAl_2O_4$) with spinel structure has a high melting point, high chemical inertness, good thermal stability, and excellent mechanical properties. Due to these properties, this material has application in electronic devices, optic industries, IR windows, solar heat absorber. $MgAl_2O_4$ spinel is processed at high temperatures to produce a dense product; hence a large grain size is obtained during sintering processes. Therefore, the drawback of the spinel ceramic is the low toughness and thermal shock resistance [1–7]. One approach to solve this problem is strengthening of $MgAl_2O_4$ spinel using Si_3N_4 nanoparticles [8,9]. Wu et al. [9] fabricated the $MgAl_2O_4$–Si_3N_4 ceramics via pressure-less sintering by using α-Si_3N_4, α-Al_2O_3, and MgO as starting materials. This group showed that the composite with 30 wt%$MgAl_2O_4$ sintered at 1620 °C has the best physical properties, excellent thermal shock resistance, suitable oxidation resistance, and good solar absorbance. Moreover, Gledhill et al. [8] successfully produced $MgAl_2O_4$–2.5vol%Si_3N_4 ceramic by the hot press technique. Their purpose was an increase in mechanical properties of $MgAl_2O_4$ spinel. The reason for using a low amount of nano-dispersoids (amorphous Si_3N_4 nanoparticles) was to keep IR-visible transparency of the bulk nanocomposite. The nanocomposite had more than 70% transparency at infrared range (3–4.5 μm). Furthermore, the results showed that after heat treatment at 1000 °C for 4 h and then cooling in the air, the tensile strength and toughness of nanocomposite were increased 29% and 85%, respectively. It is noteworthy that the optical transparency in the infrared range remained constant after the heat treatment. The formation of a compressive layer on the surface of nanocomposite is due to surface oxidation of Si_3N_4 nanoparticles [8]. However, this group only reported that the powder of nanocomposite was prepared by spray drying method without any description about the details of the experimental procedure.

To produce this nanocomposite by spray drying method, a stable suspension with a suitable pH is needed to be prepared. This suspension should be stable at least 1 h without any sedimentation. Thus, many factors such as controlling the pH, formulation, and stability of suspension are very effective to produce nanostructured granules.

The effect of ammonium polyacrylate (referred as Dolapix CE64) on the sustainability of magnesium aluminate spinel was investigated by Kadosh et al. [10]. They added 5 wt% of this dispersant agent. This addition caused a shift in spinel isoelectric point from the pH of 11.8 to 3.3. They showed that the spinel suspension in an alkaline pH (the zeta potential of −60 mV) was very stable as compared with an acidic medium (−7 mV zeta potential) [10,11]. In Albano's research [12], the effects of pH on the stability of ternary suspension (Si_3N_4 + Al_2O_3 + Y_2O_3) in the presence of ammonium polyacrylate was examined.

* Corresponding authors.
E-mail addresses: loghman57@gmail.com (M.R. Loghman-Estarki), sheikh_scientific@yahoo.com (H. Sheikh).

http://dx.doi.org/10.1016/j.ceramint.2017.06.165
Received 22 April 2017; Received in revised form 18 June 2017; Accepted 26 June 2017

Table 1
Summary of different formulations of suspension.

Sample code	Dolapix CE64 (wt%)	PVA (wt%)
S1	5	1
S2	2	1
S3	5	2
S4	2	2

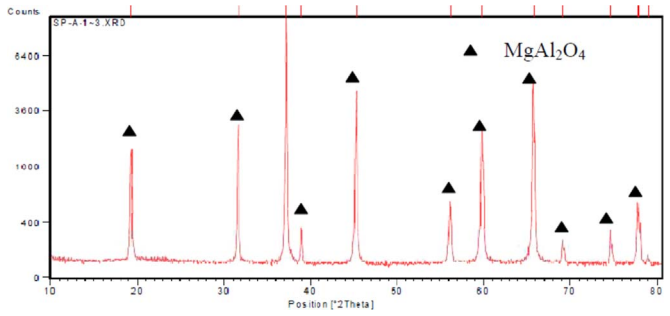

Fig. 1. The XRD pattern of $MgAl_2O_4$ nanopowders.

Alumina and yttria were used as sintering aids. They showed that the slurry containing silicon nitride, alumina and yttria nanoparticles had high stability and the minimum viscosity at pH = 9.8–10.5.

Nowadays, the ultrasonic irradiation has abundant application in the preparation of a stable suspension from metal oxide or metal nitride nanoparticles [13,14]. However, according to the best of our knowledge, there isn't any report for the preparation of $MgAl_2O_4$/2.5 vol% Si_3N_4 nanocomposite powder by using an ultrasonic treatment of its suspension. In the present work, magnesium aluminate and silicon nitride nanoparticles were dispersed in an aqueous solution in the presence of ammonium methacrylate (Dolapix CE64) with assisting the ultrasonic vibration.

2. Materials and experimental procedure

2.1. Preparation of suspensions

In a typical procedure, 20 g $MgAl_2O_4$ (purchased from Nanonovin Bahar Co.,Iran, Purity = > 99.9%), 0.49 g amorphous Si_3N_4 (purchased from Sigma-Aldrich Company) nanoparticles were mixed with two different amounts of PVA (as a binder) and polymethyl methacrylate (Dolapix CE640, as a dispersant agent) in 200 ml water to prepare different suspensions. The formulation of the used suspensions is summarized in Table 1. The pH of all suspensions was adjusted at pH=8.5 with the manual addition of appropriate amount of 1 M NaOH solution. According to the spray dryer catalog, the acidic (below pH = 6) or alkaline pH (above pH = 10) corrodes the spray dryer equipment; thus, the pH of 8.5 was selected for the suspensions. In this work, the nanoparticles were dispersed with the assistance of ultrasonic wave (TOPSONICS ultrasonic liquid processor, UP-400 series with a wave of frequency 20 ± 1 kHz and power 400 W, made in Iran) for 30 min. The lower time of ultrasonic irradiation was also tested and it was found that the suspension with different formulations was deposited rapidly. The necessary minimum time for stability of suspension is 60 min. This time is due to this fact that during suction of a suspension to the spray dryer instrument, the nanoparticles shouldn't deposit in tube or nozzle of the spray dryer at least for 60 min.

A small value of the suspensions was used to determine the zeta potential (Malvern Zeta Sizer, Zen3600). Sedimentation ratio (SR = H_S/H_i) was calculated from the height of precipitant after 120 min (H_s) and the initial height of suspension (Hi = 10 ml). For doing this test, 0.2 g nanocomposite powder and required values of PVA and Dolapix CE 64 were dispersed in 10 ml distilled water. This slurry was ultrasonicated with Topsonics (UP400-A model, Iran) for 5 min and then, was treated in another ultrasonic bath (Power Sonic405, South Korea) for 40 min. The pH of all suspensions was kept constant at 8.5 by adding aqueous ammonia. The viscosity of samples (centipoises (cp)

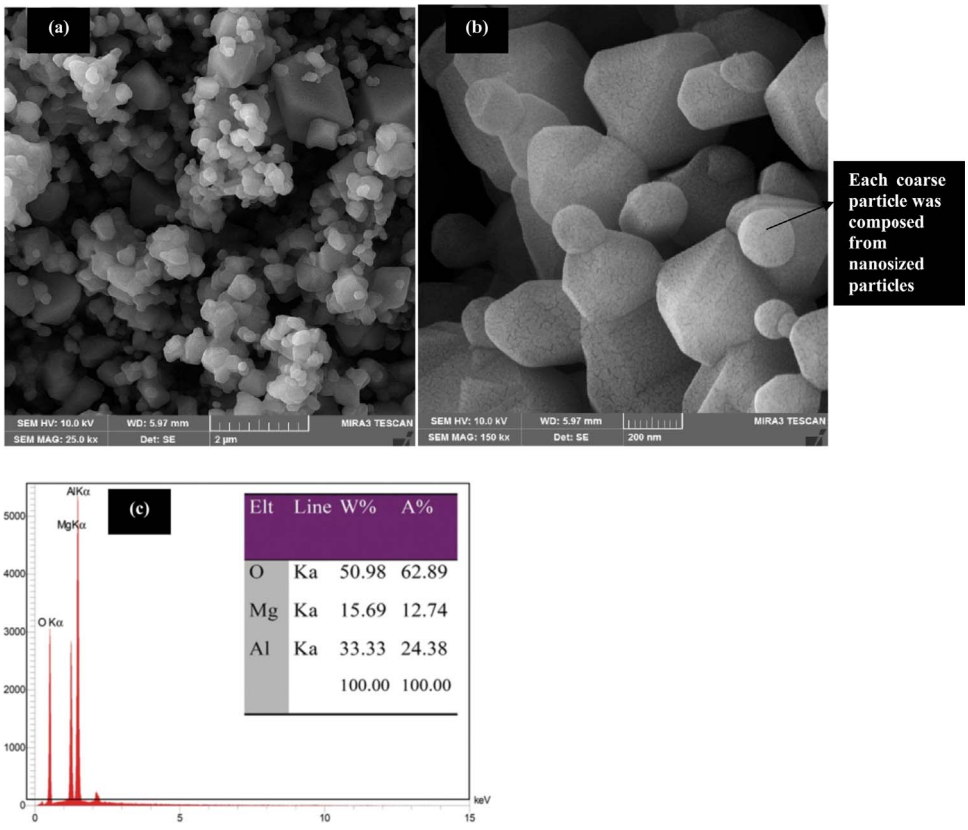

Fig. 2. (a and b) FESEM images and (c) EDS analysis of $MgAl_2O_4$ nanopowders.

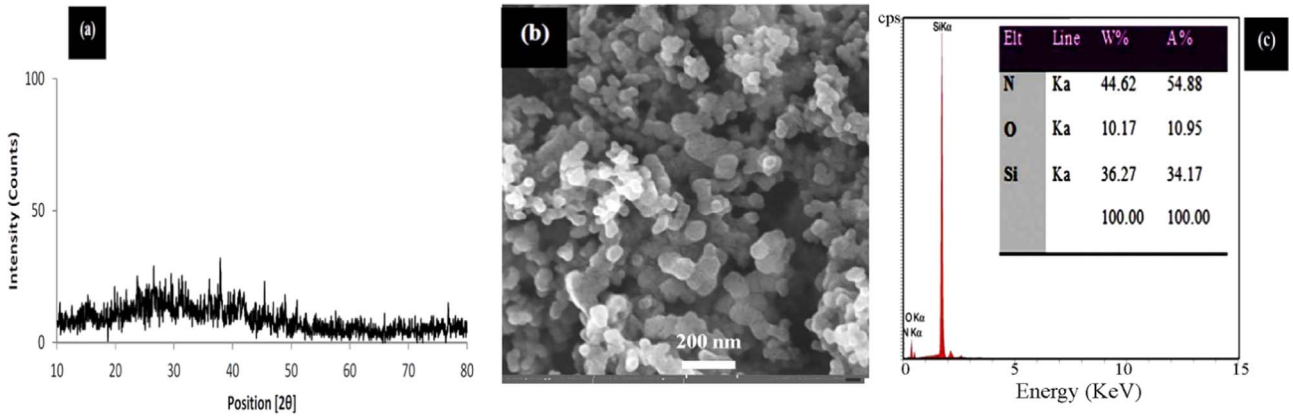

Fig. 3. (a)XRD pattern (b) FESEM image and (c) EDS analysis of Si_3N_4 nanopowders.

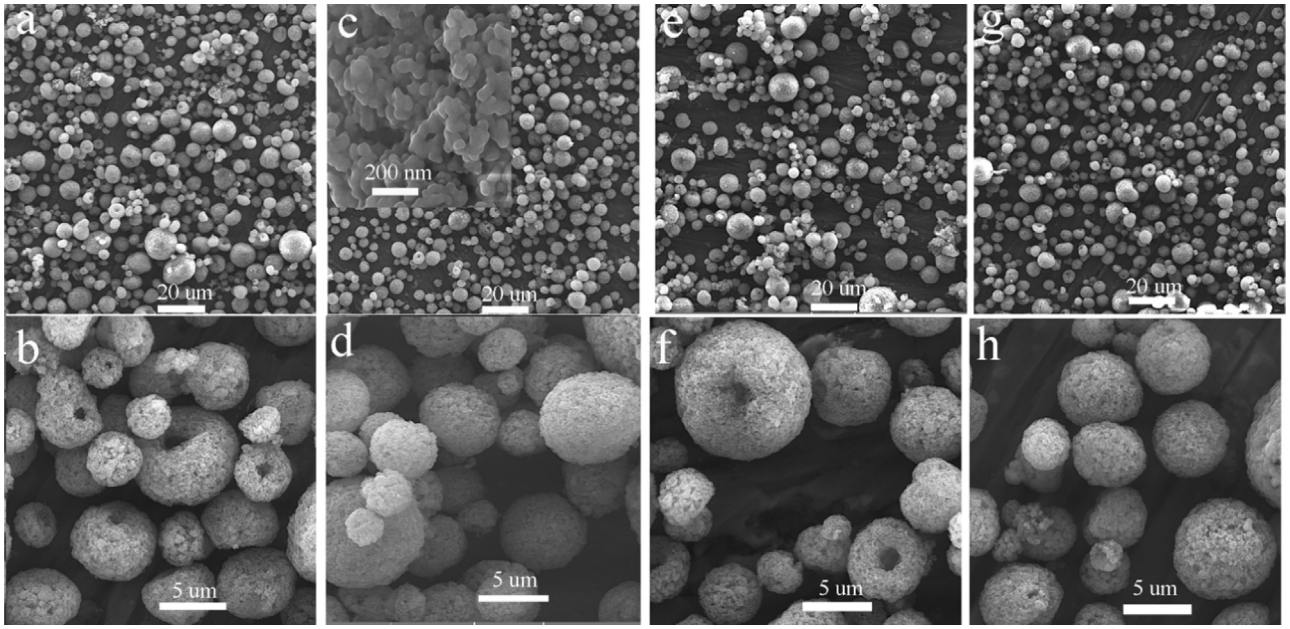

Fig. 4. FESEM images of different samples (a and b) S1,5 wt% Dolapix and 1 wt% PVA (c and d) S2, 2 wt% Dolapix and 1 wt% PVA (e and f) S3, 5 wt% Dolapix and 2 wt% PVA (g and h) S4, 2 wt% Dolapix and 2 wt% PVA (inset Fig. 4c) high magnification image of granules.

or mPa.s unit) was determined by KVS Krebs viscometer (Max Technics Co., Canada).

2.2. Preparation of granules

The as-used laboratory scale spray dryer machine is LabPlant SD Basic FT30MKIII (Keison products, Chelmsford, Essex, UK). For spray drying process, the suspensions with different amounts of binder and dispersant agent (Table 1) were spray dried into a heater chamber with an air flow of 180 °C and a rate of 3 ml/min. Thus, 200 ml suspension needs about 60 min for spray drying. Finally, the granules were collected from the cyclone chamber.

In the present work, the effect of feed rate and temperature wasn't investigated due to uncontrollable of feed rate in the as-used spray dryer machine. Also the temperature was considered as a constant parameter.

2.3. Characterization methods

X-ray diffraction (XRD) patterns were recorded on the Bruker D8 Advance X-ray diffractometer with Cu Kα (λ = 0.15406 nm). A Tescan Mira (III) field emission scanning electron microscopy (FESEM) was used to characterize the morphology and analyses of the samples. The Fourier transform infrared (FTIR) spectroscopic studies were performed using a JASCO FTIR-6300 spectrometer. The particle size distribution of different powders was measured by an image analysis method (Microstructural Image Processing (MIP) software, student version, Nahaminpardazan Company, Iran). For estimation of the average particle size and the circularity factor of granules with different suspension formulations, image analyses of FESEM images were used. These analyses were carried out at the magnification of 500X, and the count of analyzed particles was more than 1000 particles.

Inductive coupled plasma (ICP) analysis was performed by ICP Spectro Acros analyzer (AMETEK company, made in Germany).

3. Results and discussion

Fig. 1 shows the XRD pattern of $MgAl_2O_4$ nanopowders. According to this figure, all reflections are in good agreement with spinel ($MgAl_2O_4$) phase (JCPDS no. 21-1152, crystal system = cubic, a = 0.808 nm). As it is seen in Fig. 2, the spinel nanoparticles have an average size of 200 nm. A close look at Fig. 2b, it is clearly observed that each coarse particle is constituted from very fine nanosized particles (~ 30–40 nm). The EDS analysis (Fig. 2c) shows that the Mg, Al, and O exist in this sample. According to EDS analysis, the mole ratio of Mg: Al is equal to 1:2 which is good agreement with a stoichiometric formula of the spinel phase.

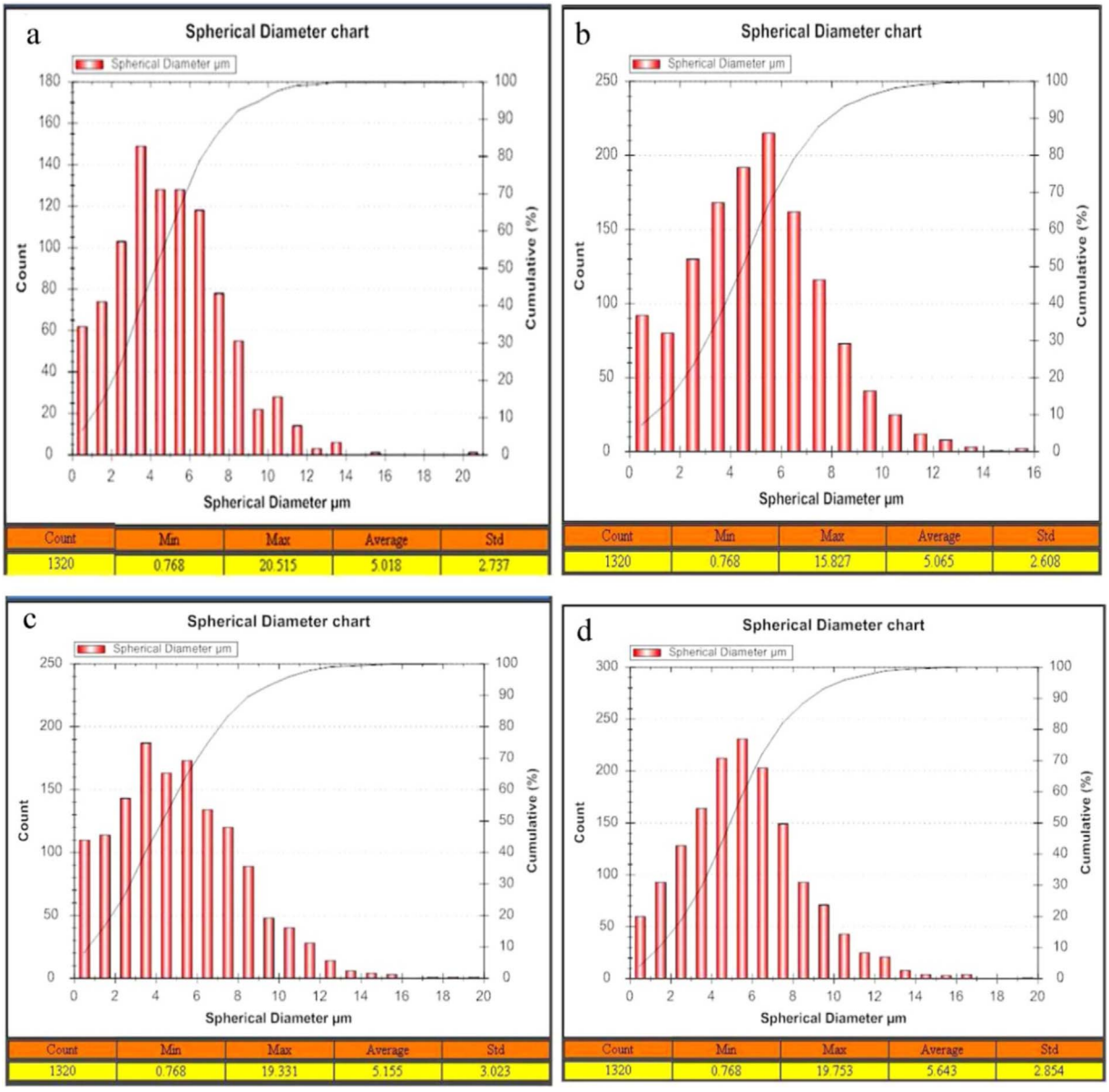

Fig. 5. Size distribution of different samples (a) S1 (b) S2 (c) S3 (d) S4.

Fig. 3a shows the XRD pattern of Si_3N_4 nanopowders. According to this figure, no obvious reflections of crystalline silicon nitride are observed; hence, this nanopowder is amorphous. As shown in FESEM image (Fig. 3b), Si_3N_4 powder includes semi-spherical nanoparticles with average size of 40–50 nm. The EDS analysis estimates that the atomic ratio between Si: N equals to 54.88:34.17 which is relatively close to the stoichiometric of silicon nitride (Si: N = 3:4). The presence of oxygen in EDS analysis is due to oxidation of amorphous Si_3N_4 nanoparticles [8,15].

Figs. 4a and e show the FESEM images of the S1 and S3 samples, respectively. According to this figures, the mixtures of spherical and doughnut-shaped morphology are obtained with 5% Dolapix and 1–2% PVA. By reducing the amount of Dolapix from 5% to 2% (at a fixed amount of binder), the majority of granules have a spherical morphology (Figs. 4d and h). Thus, for having a homogenous spherical morphology, the amount of dispersant and binder agent should be 2% and 1 or 2%, respectively. The inset of Fig. 4c shows a high magnification image of the granules. According to this figure, the granules are composed of particles with size ranging from 50 nm to 100 nm. Thus, Fig. 4 indicates that the diameter of the nanoparticles is reduced after spray drying in comparison with the initial feedstock (Fig. 2a,b). This might be attributed to the use of ultrasonic waves to disperse the nanoparticles in the suspension. In other words, ultrasonic waves lead to break the agglomerates of the spinel powder. The ultrasonic technique with acoustic cavitation generates high localized pressures and temperatures. The unique released energy can cause a temperature of ~ 5000 K and a pressure of ~ 1000 bars. Acoustic cavitation involves the formation, growth, and implosive collapse of bubbles in a liquid. This method releases the concentrated energy stored in collapsing bubbles within a very short time. That's why the ultrasound-assisted method can be adequate for agglomerates to be broken into fine nanoparticles [13,14].

Figs. 5 and 6 show the particle size distribution and circularity factor analysis of each spray dried powder, respectively. These results are summarized in Table 2. Based on image analyses, the mean particle size and the circularity of granules of are 5.0 ± 2.7 µm and 0.883 ± 0.148, respectively, for the S1 sample (Fig. 5a and Fig. 6a). By using Fig. 6a and Fig. 6b and the results of S1 and S2 samples in Table 2, it can be concluded that by reducing the amount of Dolapix from 5% to 2% (at the fixed amount of binder 1%), the circularity factor of the S2

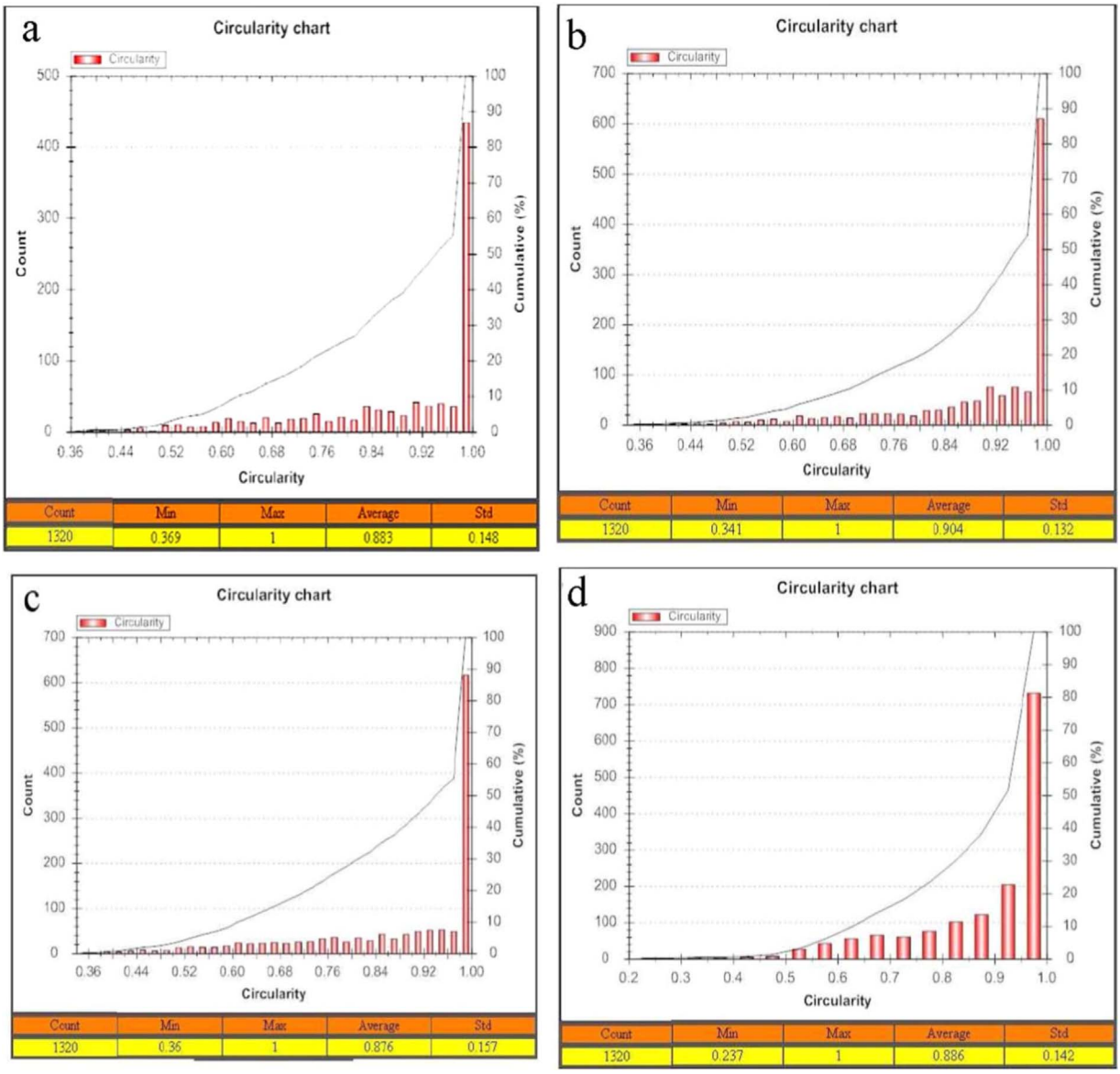

Fig. 6. Circularity of different samples (a) S1 (b) S2 (c) S3 (d) S4.

Table 2
The particle size distribution and the circularity factor of different samples.

	Average size (μm)	Average of circularity	Flow-ability (g/min)
S1	5.0 ± 2.7	0.883 ± 0.148	0.29
S2	5.1 ± 2.6	0.934 ± 0.132	0.38
S3	5.1 ± 3.0	0.876 ± 0.157	0.26
S4	5.6 ± 2.8	0.886 ± 0.142	0.30

Table 3
Zeta potential and viscosity of different suspensions.

	SR = (H_S/H_i) after 120 min	ζ (mV)	Mean Viscosity (cp or mPa s)
S1	0.25	−31.6	167
S2	0.20	−26.6	170
S3	0.20	−19.5	180
S4	0.20	−38.7	185

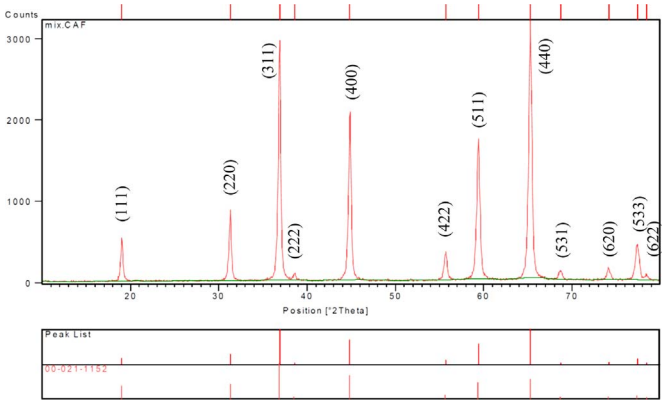

Fig. 7. The XRD pattern of $MgAl_2O_4$-Si_3N_4 nanocomposite powders.

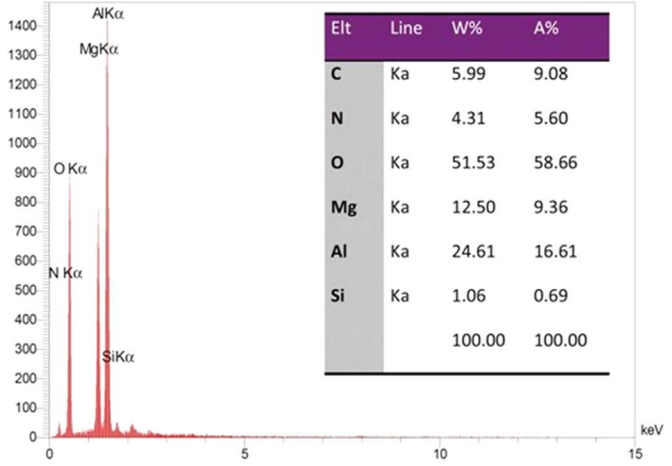

Elt	Line	W%	A%
C	Ka	5.99	9.08
N	Ka	4.31	5.60
O	Ka	51.53	58.66
Mg	Ka	12.50	9.36
Al	Ka	24.61	16.61
Si	Ka	1.06	0.69
		100.00	100.00

Fig. 8. The EDS analysis of $MgAl_2O_4$-Si_3N_4 nanocomposite powder.

sample is higher than that of the S1 sample without any significant change in diameter and standard deviation (σ) of the mean particles size.

By comparing the S2 with the S4 in Table 2, it is deduced by increasing the amount of binder from 1% to 2% (at the constant amount of Dolapix 2%), the circularity factor of the granules decreases from 0.934 to 0.886 and the mean particle size increases from 4.8 to 5.5 μm. Furthermore, the comparison of S3 with S4 points out that by reducing the amount of Dolapix from 5% to 2% (at a constant amount of binder 2%), the circularity factor (CF) and the mean particle size (d) increase (CF = 0.876 vs. 0.886, d = 5.1 μm vs. 5.6 μm). In regard to this discussion, it can be concluded that both CF and particle size can be affected by different amounts of Dolapix and PVA.

Generally, five factors affect spray dried powder characteristics including the type of atomizer, suspension components, feed speed, drying temperature and pressure of the atomizer [16]. According to the theory of spray drying [16,17], this process is a combination of complex mechanisms. The empirical equation (Eq. (1)) is used to predict the mean size diameter (SMD) for external mixing nozzles [16]:

$$SMD = C\left(\frac{\rho_L^{0.25}\eta_L^{0.06}\sigma^{0.375}}{\rho_A^{0.375}}\right)\left(\frac{\dot{m}_L}{\dot{m}_L U_L + \dot{m}_A U_A}\right)^{0.55} \quad (1)$$

where C is a fixed value depended on nozzle design, ρ, η_L, σ, $\dot{m}$ and U are density, viscosity, surface tension, flow, and speed rate of liquid (L) or air (A), respectively. As it is seen in Table 3, the viscosity of the suspensions is very close to each other. On the other hands, the power of η_L in Eq. (1) is very small. Consequently, the effect of viscosity on SMD is almost equal for all suspensions.

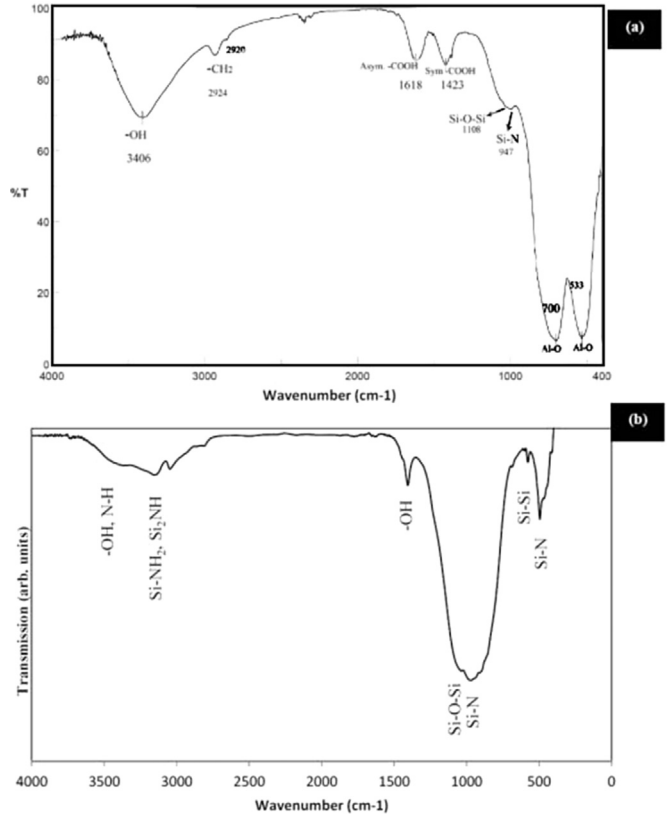

Fig. 10. FT-IR spectra of (a) as-received Si_3N_4 nanopowders and (b) spinel- silicon nitride granules.

From the suspension formulation, two effective factors on the granules morphology are the zeta potential and viscosity of the slurry. According to Ohshima's approximation [18], the changes in viscosity (η_L), electrophoresis mobility (μ_e=v/E = velocity of particle in the electrical field), and dielectric constant (or relative permittivity, ε)

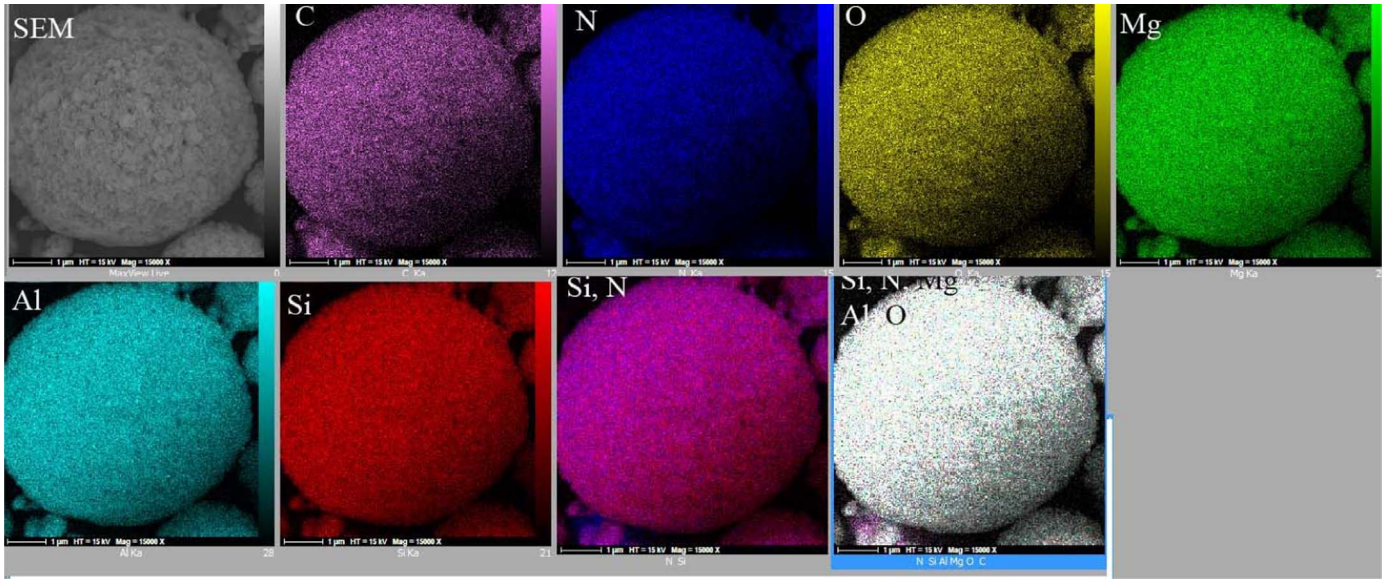

Fig. 9. EDX-mapping of $MgAl_2O_4$-Si_3N_4 nanocomposite powders.

can change the zeta potential (ζ) of suspension as following:

$$\zeta = \frac{\eta_L \mu_e}{\varepsilon} \quad (2)$$

Table 3 shows the zeta potential (ζ) of different suspension formulations. According to this table, the S4 sample has the maximum ζ value. The literature review shows that the stable (zeta potential above − 55 mV) and fluctuated suspension (zeta potential below − 40 mV) can result hollow granules and solid granules, respectively. Therefore, it is predicted that all suspensions resulted in solid sphere; because all of suspensions are flocculent type [19–23].

However, in some spray-dried suspension, the hollow sphere can be seen. It may be due to the presence of higher amount of binder that increases the viscosity of suspension and affects resulting spray-dried granules shape. According to Table 3, the sedimentation ratio (SR) decreases for the higher amount of binder. It means PVA prevents aggregation or interaction among surfaces of particles [19–23].

One of the necessary characteristics of the powders in sintering process is its high flowability. The flowability of granules depends on grain size, shape, friction between particles and moisture amount of granules. If the friction increases, powder flowability decreases. Very fine, wet or damp powder may not flow properly. If the flowability of a ceramic powder is to be at the range of 0.4–0.5 g/min (according to the standard ASTM B213-03) [24], granules are very suitable for the sintering process. From Table 3, it is found that the S2 sample has the highest flowability and low standard deviation in mean particle size. Thus, this sample was selected as an optimized sample for further characterization.

Fig. 7 shows the XRD pattern of $MgAl_2O_4$-Si_3N_4 nanostructured granules. According to this figure, all diffractions are in good agreement with the spinel ($MgAl_2O_4$) phase with JCPDS no. 21-1152 and lattice parameter of a = 0.808 nm. Due to the detection limit of XRD analysis and amorphous structure of as-used Si_3N_4 nanoparticles, it isn't expected to see any diffraction of Si_3N_4 in the XRD analysis.

Fig. 8 shows the EDS analysis of granulated powder. According to this analysis, the presence of Mg, Al, Si, N and oxygen elements demonstrate the formation of spinel/silicon nitride nanocomposite during spray drying process. The presence of carbon in this analysis is related to the carbon of binder (PVA) and dispersant agent (Dolapix). Furthermore, ICP analysis shows that the purity of the optimized sample after removing carbon by calcination treatment at 500 °C for 2 h is more than 99.9%. The small amount of impurity such as Fe (200 ppm), Na (15 ppm), Si (12 ppm), K (150 ppm) and Ca (400 ppm) is found in this sample.

Fig. 9 shows the EDX-mapping of $MgAl_2O_4$-Si_3N_4 granules. This figure illustrates that Mg, Al, Si, N and O elements have good distributions and no separated Si and N elements (from Si_3N_4 nanoparticles) are observed

Fig. 10 shows the FT-IR spectra of as-received Si_3N_4 nanopowders (Fig. 10a) and spinel- silicon nitride granules (Fig. 10b). In Fig. 10a, the stretching vibration absorption peak of symmetric and asymmetric Si–N bond in 490 cm^{-1} and 940 cm^{-1} are seen. The strong absorption peak of symmetric stretching of Si-O-Si in 1110 cm^{-1} is observed in Fig. 10a. Furthermore, the absorption peaks of hydroxyl groups (-OH), amine (Si-NH_2) and imine (Si_2NH) are visible at the range of 3500–3100 cm^{-1} [25–27]. Due to the high free surface of amorphous Si_3N_4 nanopowders [26,27], moisture in the air is adsorbed on this nanopowder. Thus, the hydroxyl group (-OH) absorption is clearly observed in FT-IR of Si_3N_4 nanopowders (Fig. 10a).

Fig. 10b shows FT-IR spectrum of spinel- silicon nitride granules. The stretching vibration absorption peak in the range of 3406 cm^{-1} is related to water or the hydroxyl group (- OH) of binder (polyvinyl alcohol) or Dolapix molecules. The symmetric and asymmetric stretching -CH_2 are observed in 2924 cm^{-1} and 2920 cm^{-1}. These peaks are related to PVA or Dolapix as a binder and dispersant agent, respectively. The absorption peaks in 1423 cm^{-1} and 1618 cm^{-1} correspond to the vibration of asymmetric and symmetric of -COOH group in the polymethyl methacrylate (Dolapix CE64). The $MgAl_2O_4$ nanoparticles have 16 phonon peaks, including $1A_{1g}$ + 1Eg + $3T_{2g}$ + $4T_{1u}$ + T_{1g} + $2A_{2u}$ + $2E_u$ + $2T_{2u}$. Among these peaks, A_{1g}, E_g, and T_{2g} are active in Raman analysis and four peaks of T_{1u} mode are active in IR analysis. In the FT-IR of granules, two stretching frequencies in the range of 1500–700 cm^{-1} belong to the tetrahedral and octahedral vibration of Al–O bonds. This peak corresponds to T1u mode in AlO6 unit that is the structural unit of the spinel network [28,29]. In addition, the absorption peaks in 1108 cm^{-1} and 947 cm^{-1} confirm the presence of silicon nitride in the nanocomposite granules with Si–O bonds [28–30].

4. Conclusion

In summary, it can be concluded that ultrasonic vibration can lead to a fine particle size of spinel particles and a stable suspension for spray drying. The test of zeta potential determination shows that all suspensions are flocculent type; hence the solid granules are produced during spray drying of the suspensions. Also, the optimum formulation for the production of spinel-silicon nitride nanocomposite, which can be used in the sintering process, was obtained with 1 wt% binder (PVA) and 2 wt% Dolapix. The optimal powder had a size distribution of 5.1 ± 2.6 μm and the circularity coefficient of 0.934 ± 0.132 with good flowability (0.39 g/min).

Acknowledgment

The author should have thank from Iran National Foundation (INSF, Grant no. 95841433) and Malek Ashtar University of Technology for financial support of this project

References

[1] M. Rubat Merac, The role of impurities, LiF, and processing on the sintering, microstructure, and optical properties of transparent polycrystalline magnesium aluminate (MgAl2O4) Spinel, Colorado School, 2013.
[2] L.B. Kong, Y. Huang, W. Que, T. Zhang, D.,J. Zhang, D. Tang, Transparent Ceramics, Springer, 2015.
[3] A. Goldstein, Correlation between MgAl2O4.spinel structure, processing factors and functional properties of transparent parts, J. Eur. Ceram. Soc. 32 (2012) 2869–2886.
[4] S. Cooper, C. Hodson, Magnesia-magnesium aluminate spinel as a refractory, Trans. J. Br. Ceram. Soc. 81 (1982) 121–128.
[5] B.C. Smith, Fundamentals of Fourier Transform Infrared Spectroscopy, CRC Press, Hoboken, 2011.
[6] K. Maca, M. Trunec, R. Chmelik, Processing and properties of fine-grained transparent $MgAl_2O_4$ ceramics, Ceramics Silikáty 51 (2007) 94–97.
[7] S.F. Wang, J. Zhang, D. Luo, W. Gua, Tang, D.Y. Dong, Z.L. Tan, X. Que, T.S. Zhang, Transparent ceramics: processing, materials and applications, Prog. Solid State Chem. 41 (2013) 20–54.
[8] A.D. Gledhill, D. Li, T. Mroz, Strengthening of transparent Spinel/Si_3N_4 nanocomposites, Acta Mater. 60 (2012) 1570–1575.
[9] J.f. Wu, Y. Zhang, X. Xu, T. Deng, X. Lao, K. Li, X. Xu, Thermal shock resistance and oxidation behavior of in-situ synthesized $MgAl_2O_4$–Si_3N_4 composites used for solar heat absorber, Ceram. Int. 42 (2016) 10175–10183.
[10] T. Kadosh, Y. Cohen, Y. Talmonand, W.,D. Kaplan, In situ characterization of spinel nanoceramic suspensions, J. Am. Ceram. Soc. 95 (2012) 3103–3108.
[11] P. Albano, B. Garrido, Processing of concentrated aqueous silicon nitride slips by slip casting, J. Am. Ceram. Soc. 81 (1998) 837–844.
[12] P. Albano, B. Garrido, Processing of Concentrated Aqueous Si_3N_4 Slips Stabilized With Tetramethylammonium Hydroxide 8, ASM International, 1999, pp. 184–189.
[13] K. Nogo, W. Qi, K. Mori, S. Ogawa, D. Inohara, S. Hosono, N. Kawashima, A. Nishiyama, K. Wada, I. Ishimaru, Ultrasonic separation of a suspension for in situ spectroscopic imaging, Opt. Rev. 23 (2016) 360–363.
[14] K. Sato, J. Guang Li, H. K, Takamasa Ishigaki, Ultrasonic dispersion of TiO_2 nanoparticles in aqueous suspension, J. Am. Ceram. Soc. 91 (2008) 2481–2487.
[15] J.B. Wen, S. Huang, H.J. Wang, Oxidation behavior of amorphous nano-Si3N4 powders, Key Eng. Mater. 602–603 (2014) 367–370.
[16] S.J. Lukasiewicz, Spray-drying ceramic powders, J. Am. Ceram. Soc. 72 (4) (1989) 617–624.
[17] X.Q. Cao, R. Vassen, S. Schwartz, W. Jungen, F. Tietz, D. Stöever, Spray-drying of ceramics for plasma-spray coating, J. Eur. Ceram. Soc. 20 (2000) 2433–2439.
[18] H. Ohshima, A simple expression for Henry'S function for the retardation effect in electrophoresis of spherical colloidal particles, J. Colloid Interface Sci. 168 (1994) 269–271.

[19] H. Mahdjoub, P. Roy, C. Filiatre, G. Bertrand, C. Coddet, The effect of the slurry formulation upon the morphology of spray-dried yttria stabilised zirconia particles, J. Eur. Ceram. Soc. 23 (2003) (1637–164).
[20] G. Bertrand, C. Coddet, Spray drying and sintering of zirconia based hollow powders Priscille Roy, Powder Technol. 157 (2005) 20–26.
[21] G. Bertrand, P. Roy, C. Filiatre, C. Coddet, Spray-dried ceramic powders: a quantitative correlation between slurry characteristics and shapes of the granules, Chem. Eng. Sci. 60 (2005) 95–102.
[22] W.J. Jr. Walker, J.S. Reed, S.K. Verma, Influence of slurry parameters on the characteristics of spray-dried granules, J. Am. Ceram. Soc. 82 (7) (1999) 1711–1719.
[23] A. Stunda-Zujeva, Z. Irbe, L. Berzina- Cimdina, Controlling the morphology of ceramic and composite powders obtained via spray drying – a review, Ceram. Int. (2017). http://dx.doi.org/10.1016/j.ceramint.2017.05.023.
[24] ASTM B213-03, Standard Test Method for Flow Rate of Metal Powders, ASTM International, West Conshohocken, PA, 2003.
[25] N. Wada, S.A. Solin, J. Wong, S. Prochazka, Raman and IR absorption spectroscopic studies on α, β, and amorphous Si3N4, J. Non-Cryst. Solids 43 (1981) 7–15.
[26] Kirill O. Bugaev, Anastasia A. Zelenina, Vladimir A. Volodin, Vibrational spectroscopy of chemical species in silicon and silicon-rich nitride thin films, Int. J. Spectrosc., 2012. Article ID 281851, p. 5.
[27] N. Wada, S.A. Solin, J. Wong, S. prochazka, ramanand ir absorption spectroscopic studies on a, ~, and amorphous Si_3N_4, J. Non-Cryst. Solids 43 (1981) 7–15.
[28] M.Y. Nassar, I.S. Ahmed, I. Samir, A novel synthetic route for magnesium aluminate ($MgAl_2O_4$) nanoparticles using sol–gel auto combustion method and their photocatalytic properties, Spectrochim. Acta Part A: Mol. Biomol. Spectrosc. 131 (2014) 329–334.
[29] P.Y. Lee, H. Suematsu, T. Yano, K. Yatsui, Synthesis and characterization of nanocrystalline $MgAl_2O_4$ spinel by polymerized complex method, J. Nanopart. Res. 8 (2006) 911–917.
[30] J. Chandradass, K.H. Kim, Effect of precursor ratios on the synthesis of $MgAl_2O_4$ nanoparticles by a reverse microemulsion method, J. Ceram. Proc. Res. 11 (2010) 96–99.